

Bifurcation structures in maps of Hénon type

Kai T Hansen^{†§} and Predrag Cvitanović^{‡||}

[†] NORDITA, Blegdamsvej 17, DK-2100 Copenhagen Ø, Denmark

[‡] Center for Chaos and Turbulence Studies, Niels Bohr Institute, Blegdamsvej 17, DK-2100 Copenhagen Ø, Denmark

Received 9 May 1997

Recommended by P Grassberger

Abstract. We construct a series of n -unimodal approximations to maps of the Hénon type and utilize the associated symbolic dynamics to describe the possible bifurcation structures for such maps. We construct the bifurcation surfaces of the short periodic orbits in the topological parameter space and check numerically that the Hénon map parameter plane (a, b) is topologically equivalent to a two-dimensional section through the infinite-dimensional parameter space characterizing a generic map of the Hénon type.

PACS numbers: 0320I, 0545B

1. Introduction

While the topological dynamics of unimodal and multimodal one-dimensional mappings is well understood [30, 28], a classification of all possible topologically distinct dynamical systems in two or more dimensions remains an open problem. The goal of this paper is to develop a theory of bifurcation diagrams which classify and order topologically distinct bifurcation sequences for two-dimensional invertible maps of the Hénon type [20]. We consider maps which stretch and fold the phase space once under one mapping, exemplified by a Smale horseshoe [33]. We study here the maps which *do not* have a complete binary Cantor set repeller such as a complete horseshoe map has, but assume that the admissible orbits can still be uniquely identified by a subset of the binary symbolic dynamics itineraries [12, 13, 7]. This assumption has not been proved for the Hénon map, but is supported by all of our numerical results.

The Hénon map [20] is an invertible mapping of a two-dimensional plane into itself:

$$\begin{aligned}x_{t+1} &= 1 - ax_t^2 + y_t \\ y_{t+1} &= bx_t.\end{aligned}$$

Equivalently, the Hénon map can be defined by the 2-step recurrence relation

$$x_{t+1} = 1 - ax_t^2 + bx_{t-1}. \quad (1)$$

The Hénon map is one of the simplest models of a Poincaré map of a three-dimensional invertible flow. Our description of the bifurcation diagram for all maps of the Hénon type

[§] Present address: ABB Corporate Research, PO Box 90, N-1361 Billingstad, Norway. E-mail: khansen@nordita.dk

^{||} Also at: Department of Physics and Astronomy, Northwestern University, 2145 Sheridan Road, Evanston, IL 60208-3112, USA. E-mail: predrag@nbi.dk

(once-folding maps) will be generic in the sense that it will be valid for all flows which fold the phase space at most once between subsequent Poincaré sections.

Detailed numerical investigations of such structures for the Hénon map have been carried out by Mira and co-workers [8, 29, 5], as well as many other authors [1, 2–4, 12, 13, 15, 20, 27, 29, 32], to cite but a few. Our approach is different in so far that instead of studying the bifurcation structure of the Hénon map or the Lozi map [22], we offer here a topological characterization of the parameter space and the admissible orbits for all maps of the Hénon type. The approach is closely related to the pruning front conjecture [7, 6]. There the phase space stable–unstable manifolds foliations are replaced by a straightened-out symbol plane ‘street map’ applicable to any map of the Hénon type. The totality of all turning points of the unstable manifold of the map delineates the ‘pruning front’ in the symbol plane, the border between the admissible and inadmissible orbits. For unimodal one-dimensional mappings the pruning front is specified by a single parameter, the ‘kneading invariant’ [30, 28], but for two-dimensional mappings infinitely many parameters are required to specify the pruning front, that is to say the infinity of the turning points of the unstable manifold.

However, one striking feature of smooth dissipative once-folding maps is their hierarchic foliation; for small values of the modulus of b in coarsest resolution they look like unimodal maps, under somewhat finer resolution two primary folds are discernible, and so forth. This observation is the basis for a systematic approximation to two-dimensional once-folding maps by sequences of n -unimodal one-dimensional maps that we shall develop here; we shall construct nested sequences of parameter topological ‘street maps’ of all admissible (but strongly hierarchically ordered) parametrizations of once-folding maps. A symbol plane together with a pruning front specifies symbolic dynamics of a *given* once-folding map; our n -unimodal approximation to describes *all* admissible once-folding maps, with a point in the topological parameter space corresponding to a particular topological parameter.

The bifurcation theory presented here is based on [16], and the bifurcation structures in multi-unimodal one-dimensional maps are discussed in the spirit of the work in [18].

2. Unimodal approximation

In the $b \rightarrow 0$ limit the unstable manifold of the Hénon map shrinks to a one-dimensional arc, folds of the stable manifold stretch off to infinity, and the Hénon map (1) reduces to the one-dimensional quadratic map

$$x_{t+1} = 1 - ax_t^2 \quad (2)$$

with one critical point $x_c = 0$.

The symbolic description for a unimodal map with a critical point x_c is defined by

$$s_t = \begin{cases} 1 & \text{if } x_t > x_c \\ 0 & \text{if } x_t < x_c. \end{cases} \quad (3)$$

The infinite symbol sequence $S(x) = s_1 s_2 s_3 \dots$ is the (*future*) *itinerary* of the point $x = x_0$. The dynamics acts on this sequence as a shift:

$$S(f^t(x)) = \sigma^t S(x) = s_{1+t} s_{2+t} s_{3+t} \dots \quad (4)$$

Symbols L and R are often used [26] instead of 0 and 1, indicating that the point x_t lies either to the left or right of the critical point. The critical point x_c may be denoted by $s_t = C$.

To any given itinerary S we associate the point $\gamma(S) \in [0, 1]$ constructed as follows

$$w_{t+1} = \begin{cases} w_t & \text{if } s_{t+1} = 0 \\ 1 - w_t & \text{if } s_{t+1} = 1 \end{cases} \quad w_1 = s_1$$

$$\gamma(S) = 0.w_1w_2w_3\dots = \sum_{t=1}^{\infty} w_t/2^t.$$
(5)

The number $\gamma(S)$ is independent of details of a particular unimodal map and preserves the ordering of x in the sense that if $\hat{x} > x$ then $\gamma(S(\hat{x})) > \gamma(S(x))$ for any unimodal map. We shall refer to $\gamma(S)$ as the *(future) topological coordinate* or the *(future) symbolic coordinate*.

2.1. Kneading values

If the parameter in the quadratic map (2) is $a > 2$ then the iterates of the critical point x_c diverge for $t \rightarrow \infty$. As long as $a \geq 2$, any sequence S composed of letters $s_i \in \{0, 1\}$ is admissible, and any value of $0 \leq \gamma < 1$ corresponds to an admissible orbit in the non-wandering set of the map. The corresponding repeller is a complete binary Cantor set.

For $a < 2$ only a subset of the points in the interval $\gamma \in [0, 1]$ corresponds to admissible orbits. The forbidden symbolic values are determined by observing that the largest x_t value in an orbit $x_1 \rightarrow x_2 \rightarrow x_3 \rightarrow \dots$ has to be smaller than or equal to the image of the critical point, *the critical value* $f(x_c)$. Let $K = S(x_c)$ be the itinerary of the critical point $x_0 = x_c$, denoting the *kneading sequence* of the map. The corresponding topological coordinate is called the *kneading value* [28]

$$\kappa = \gamma(K) = \gamma(S(x_c)).$$
(6)

If $\gamma(S) > \gamma(K)$, the point x whose itinerary is S would have $x > f(x_c)$ and cannot be an admissible orbit. Let

$$\hat{\gamma}(S) = \sup_m \gamma(\sigma^m(S))$$
(7)

be the *maximal value*, the highest topological coordinate reached by the orbit $x_1 \rightarrow x_2 \rightarrow x_3 \rightarrow \dots$.

Theorem 1 ([31, 26, 14, 30, 28]). *Let κ be the kneading value of the critical point, and $\hat{\gamma}(S)$ be the maximal value of the orbit S . Then the orbit S is admissible if and only if $\hat{\gamma}(S) \leq \kappa$.*

We shall call the interval $(\kappa, 1]$ the *primary pruned interval*. The orbit S is inadmissible if γ of any shifted sequence of S falls into this interval.

While a unimodal map may depend on many arbitrarily chosen parameters, its dynamics determines and is determined by a unique kneading value κ . There exists a map from the parameter a of a specific unimodal map to the κ -line, and thus we can use κ to parametrize any unimodal map. We shall call κ the *topological parameter* of the map. The jumps in κ as a function of a correspond to inadmissible values of the topological parameter. Each jump in κ corresponds to a stability window associated with a stable cycle of a smooth unimodal map. For the quadratic map (2) κ increases monotonically with the parameter a , but in general such monotonicity need not be the case.

2.2. Periodic orbits

A *periodic point* (or a *cycle point*) x_i belonging to a cycle of period n is a real solution of

$$f^n(x_i) = x_i, \quad i = 0, 1, \dots, n - 1, \quad f^r(x_i) \neq x_i \quad \text{for } r < n.$$
(8)

Table 1. The maximal values of unimodal map cycles up to length 5.

S	$\hat{\gamma}(S)$
$\overline{0}$	$0.\overline{0} = 0$
$\overline{1}$	$0.\overline{10} = \frac{2}{3}$
$\overline{10}$	$0.\overline{1100} = \frac{4}{5}$
$\overline{101}$	$0.\overline{110} = \frac{6}{7}$
$\overline{100}$	$0.\overline{111000} = \frac{8}{9}$
$\overline{1011}$	$0.\overline{11010010} = \frac{14}{17}$
$\overline{1001}$	$0.\overline{1110} = \frac{14}{15}$
$\overline{1000}$	$0.\overline{11110000} = \frac{16}{17}$
$\overline{10111}$	$0.\overline{11010} = \frac{26}{31}$
$\overline{10110}$	$0.\overline{1101100100} = \frac{28}{33}$
$\overline{10010}$	$0.\overline{11100} = \frac{28}{31}$
$\overline{10011}$	$0.\overline{1110100010} = \frac{10}{11}$
$\overline{10001}$	$0.\overline{11110} = \frac{30}{31}$
$\overline{10000}$	$0.\overline{1111100000} = \frac{32}{33}$

The n th iterate of a unimodal map crosses the diagonal at most 2^n times. Similarly, the backward and forward Smale horseshoes intersect at most 2^n times, and therefore there will be 2^n or fewer periodic points of length n . A cycle of length n corresponds to an infinite repetition of a length n symbol string, customarily indicated by a line over the string:

$$S = (s_1 s_2 s_3 \dots s_n)^\infty = \overline{s_1 s_2 s_3 \dots s_n}.$$

If $\overline{s_1 s_2 \dots s_n}$ is the symbol string associated with x_0 , its cyclic permutation $\overline{s_k s_{k+1} \dots s_n s_1 \dots s_{k-1}}$ corresponds to the point x_{k-1} in the same cycle. A cycle p is called *prime* if its itinerary S cannot be written as a repetition of a shorter block S' .

A cycle of a differentiable one-dimensional map is stable if

$$\left| \frac{d}{dx} f^n(x_1) \right| = |f'(x_n) f'(x_{n-1}) \dots f'(x_2) f'(x_1)| < 1.$$

A cycle is *superstable* if the above product vanishes, i.e. if the orbit includes a critical point. The interval of parameter values for which a cycle p is stable is called the stability window of p .

Each cycle yields n rational values of γ . It follows from (5) that if the repeating string s_1, s_2, \dots, s_n contains an odd number of 1's, the string of well-ordered symbols $w_1 w_2 \dots w_n$ has to be of the double length before it repeats itself. The value γ is a geometrical sum which we can write as the finite sum

$$\gamma(\overline{s_1 s_2 \dots s_n}) = \frac{2^{2n}}{2^{2n} - 1} \sum_{t=1}^{2n} w_t / 2^t.$$

Using this we can calculate the $\hat{\gamma}(S)$ for all short cycles. For orbits up to length 5 this is done in table 1.

2.3. Bifurcations

Periodic orbits in smooth unimodal maps are generically created either as a pair with one stable and one unstable length n orbit in a saddle-node bifurcation point, or as a period $2n$ orbit in a period-doubling bifurcation where a period n orbit becomes unstable.

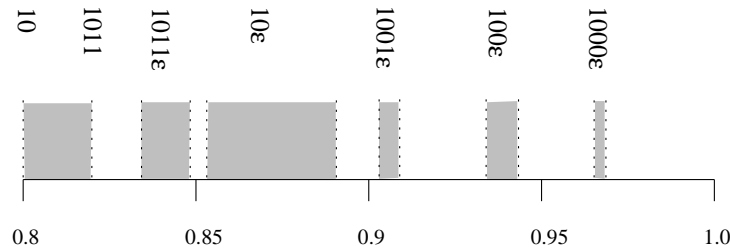


Figure 1. Bifurcation points from table 1 plotted as a function of the topological parameter κ . Grey areas are inadmissible intervals of κ corresponding to stable windows in a smooth unimodal map. As a shorthand notation for pairs of orbits we use the letter ϵ to denote either a 0 or a 1. The line over the symbol strings is omitted.

Immediately after a saddle-node bifurcation the two created orbits both have the same itinerary $\overline{s_1 s_2 \dots s_n}$ with an even number of 1's and with the topological parameter value $\kappa(\overline{s_1 s_2 \dots s_n}) = \hat{\gamma}(\overline{s_1 s_2 \dots s_n})$. Orbits with this itinerary exist for all unimodal maps with $\kappa \geq \hat{\gamma}(\overline{s_1 s_2 \dots s_n})$. As the parameter in the smooth unimodal map increases the stable orbit passes a superstable point and changes its symbolic dynamics. If we now assume that the symbol string $\overline{s_1 s_2 \dots s_n}$ is the cyclic permutation giving the maximum γ value, then the itinerary of the stable orbit after the superstable point is $\overline{s_1 s_2 \dots s_{n-1} (1 - s_n)}$, since the point closest to the critical point passes through the critical point. The topological parameter value of the map is then $\kappa(\overline{s_1 s_2 \dots s_{n-1} (1 - s_n)})$. The inadmissible topological parameter interval $(\kappa(\overline{s_1 s_2 \dots s_n}), \kappa(\overline{s_1 s_2 \dots s_{n-1} (1 - s_n)}))$ is then uniquely related to the parameter interval in a between the saddle-point bifurcation and the superstable point, or more loosely speaking; to the a interval where the orbit $\overline{s_1 s_2 \dots s_{n-1} (1 - s_n)}$ is stable.

In the same way there will be an interval

$$(\kappa(\overline{s_1 s_2 \dots s_{n-1} (1 - s_n)}), \kappa(\overline{s_1 s_2 \dots s_{n-1} (1 - s_n) s_1 s_2 \dots s_n}))$$

corresponding to the interval in a from where the orbit $\overline{s_1 s_2 \dots s_{n-1} (1 - s_n)}$ is superstable to the point where the orbit $\overline{s_1 s_2 \dots s_{n-1} (1 - s_n) s_1 s_2 \dots s_n}$ is superstable. This interval includes the period-doubling bifurcation where the $2n$ orbit $\overline{s_1 s_2 \dots s_{n-1} (1 - s_n) s_1 s_2 \dots s_n}$ is created.

From table 1 we can find some of the largest intervals in κ corresponding to the stability windows in a smooth unimodal map. The stable period 3 orbit window on the parameter a -axis corresponds to the interval $(\frac{6}{7}, \frac{8}{9})$ on the κ line and so on, see figure 1.

3. Bi-unimodal approximation

The unimodal approximation is an exact description for the Hénon map for $|b| \rightarrow 0$, but not very accurate for $b \neq 0$. We therefore continue to the next order of refinement and approximate the unstable manifold in figure 2(a) with two unimodal maps, one above the other, as sketched in figure 2(b).

It is important to note that the points in the orbit are forced to be on one of the two functions in figure 2(b) depending on one symbol in the past itinerary: if an orbit has a point on the right-hand side of the horseshoe (symbol 1) then its image is on the upper function and if an orbit has a point on the left-hand side of the horseshoe (symbol 0) then its image is on the lower function. This is illustrated in figure 2 where we have drawn the unstable manifold of the Hénon map ($a = 1.4, b = 0.3$) and one period 7 orbit. For each point in the orbit we have written the future itinerary of the point (omitting the line over the

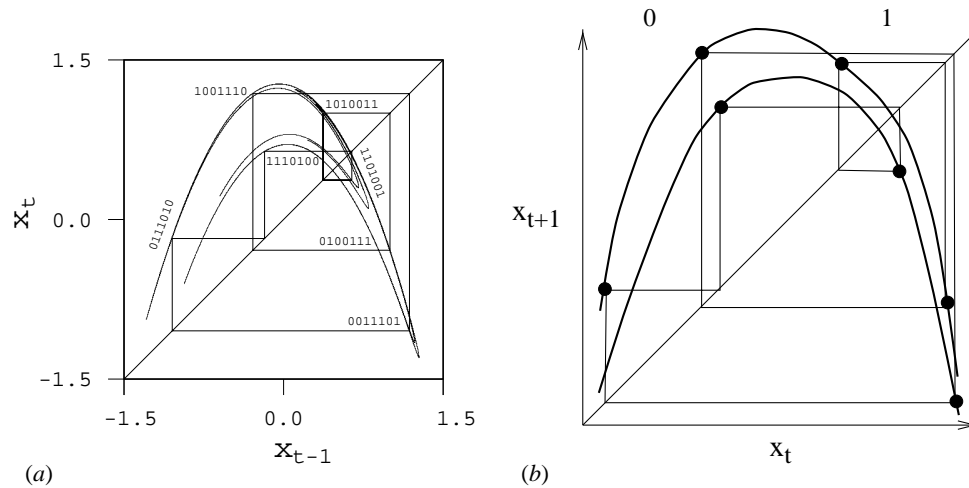


Figure 2. (a) The strange attractor (unstable manifold) and a period 7 orbit in the Hénon map ($a = 1.4, b = 0.3$). (b) A sketch of a bi-unimodal approximation with the same periodic orbit.

symbols). The choice between the upper and lower half of the unstable manifold depends on the preceding point in the orbit, and hence on the next to last symbol in the symbol string labelling the point.

We stress that this map, constructed from two unimodal maps, is *not* a multivalued map, since each point is assigned a unique value. We denote this one-dimensional map ‘bi-unimodal’ instead of bimodal not to confuse it with other bimodal maps frequently studied in the literature, such as the cubic map.

A point in an orbit with itinerary $S = \dots s_{t-2}s_{t-1}s_t \cdot s_{t+1}s_{t+2} \dots$ is mapped in the bi-unimodal approximation by the one-dimensional map

$$x_{t+1} = f_{s_{t-1}}(x_t) = \begin{cases} f_0(x_t) & \text{if } s_{t-1} = 0 \\ f_1(x_t) & \text{if } s_{t-1} = 1. \end{cases} \tag{9}$$

The two critical points of the functions f_0 and f_1 yield the two kneading sequences K_0 and K_1 , with the corresponding topological parameter values κ_0 and κ_1 . The bi-unimodal map f_s is described by the point (κ_0, κ_1) in the two-dimensional topological parameter plane. For an order-reversing two-dimensional map which flips, stretches, and folds the phase space, the critical value of f_1 is larger than that of f_0 , $\kappa_1 > \kappa_0$. This is the case for the Hénon map with $b > 0$. For an order-preserving mapping which stretches and folds without flipping the critical value of f_1 is smaller than f_0 and $\kappa_1 < \kappa_0$. This is the case for the Hénon map with $b < 0$. The line $b = 0$ is mapped into the line $\kappa_1 = \kappa_0$, the unimodal map discussed above.

We shall now trace out some of the characteristic bifurcation structures for the bi-unimodal approximation in this two-dimensional topological parameter plane.

Each orbit (except the two fixed points $\bar{0}$ and $\bar{1}$) has two maximal values $\hat{\gamma}_0$ and $\hat{\gamma}_1$ defined as for the unimodal map (7), but with the restriction that the symbol s_{m-1} is equal to the index of $\hat{\gamma}$. If the orbit is given by the itinerary $S = \dots s_{-2}s_{-1}s_0 \cdot s_1s_2 \dots$ we have

$$\hat{\gamma}_s(S) = \sup_m \gamma(\sigma^m(S)) \quad \text{with } s_{m-1} = s \tag{10}$$

where σ is the shift (4). An orbit S is admissible if and only if

$$\begin{aligned} \hat{\gamma}_0(S) &\leq \kappa_0 \\ \hat{\gamma}_1(S) &\leq \kappa_1 \end{aligned} \tag{11}$$

so the orbit S exists within a rectangle in the (κ_0, κ_1) plane. The parameter point $\kappa_0 = 1, \kappa_1 = 1$ corresponds to a complete Smale horseshoe for which all orbits exist.

In order to have a bi-unimodal map, we have to require that the images of the critical points are not above the smallest critical point. In terms of kneading sequences this constrains κ_s to

$$\kappa_s = \gamma(K_s) \geq \gamma(\sigma(K_s)) \tag{12}$$

which is true if

$$\kappa_s \geq 0.\overline{10} = \frac{2}{3}. \tag{13}$$

This requirement is less constraining in higher-order multi-unimodal approximations.

3.1. Maximal values of short cycles

We can now proceed to determine all cycles up to a given length and determine the topological values $\hat{\gamma}_s(\bar{S})$ of all their cycle points.

The fixed point $\bar{0}$ has $s_{-1} = 0$, with the only maximal value $\hat{\gamma}_0(\bar{0}) = 0$. This fixed point exists for

$$\kappa_0 \geq \hat{\gamma}_0(\bar{0}) = 0.$$

In other words, if there is anything in the non-wandering set, the fixed point $\bar{0}$ exists. The fixed point $\bar{1}$ has $s_{-1} = 1$, with the corresponding topological coordinate $\hat{\gamma}_1(\bar{1}) = 0.\overline{10}$. It exists for topological parameter plane values

$$\kappa_1 \geq \hat{\gamma}_1(\bar{1}) = 0.\overline{10} = \frac{2}{3}.$$

The 2-cycle $\overline{10}$ has two cyclic permutations. Cycle point $x_{\overline{10}}$ with itinerary $\overline{s_1 s_2} = \overline{10}$ has $s_0 = s_2 = 0$ and $s_{-1} = s_1 = 1$ giving the maximal value $\hat{\gamma}_1(\overline{10}) = 0.\overline{1100}$. The second point in the period 2 orbit, $x_{\overline{01}}$, is on map f_0 since $s_{-1} = 0$ and the maximal value is $\hat{\gamma}_0(\overline{01}) = 0.\overline{0110}$. Thus this orbit exists for the topological parameter values

$$\begin{aligned} \kappa_0 &\geq \hat{\gamma}_0(\overline{10}) = 0.\overline{0110} = \frac{2}{5} \\ \kappa_1 &\geq \hat{\gamma}_1(\overline{10}) = 0.\overline{1100} = \frac{4}{5}. \end{aligned} \tag{14}$$

There are two 3-cycles, $\overline{100}$ and $\overline{101}$ with $s_{-1} = s_2$ determining the fold to which a cycle point belongs. The $\overline{100}$ -cycle cycle points have the following topological coordinates: $\gamma_0(\overline{100}) = 0.\overline{111000}$, $\gamma_1(\overline{010}) = 0.\overline{011100}$, $\gamma_0(\overline{001}) = 0.\overline{001110}$. The two maximal values are $\hat{\gamma}_0(\overline{100})$ and $\hat{\gamma}_1(\overline{100})$, so the region in the topological parameter plane for which $\overline{100}$ exists is given by

$$\begin{aligned} \kappa_0 &\geq \hat{\gamma}_0(\overline{100}) = 0.\overline{111000} = \frac{8}{9} \\ \kappa_1 &\geq \hat{\gamma}_1(\overline{100}) = 0.\overline{011100} = \frac{4}{9}. \end{aligned} \tag{15}$$

The topological coordinates of the other 3-cycle cycle points are $\gamma_0(\overline{101}) = 0.\overline{110}$, $\gamma_1(\overline{110}) = 0.\overline{100}$, $\gamma_1(\overline{011}) = 0.\overline{010}$, so the cycle exists for

$$\begin{aligned} \kappa_0 &\geq \hat{\gamma}_0(\overline{101}) = 0.\overline{110} = \frac{6}{7} \\ \kappa_1 &\geq \hat{\gamma}_1(\overline{101}) = 0.\overline{100} = \frac{4}{7}. \end{aligned} \tag{16}$$

Table 2. The maximal values of short cycles of the bi-unimodal map.

S	$\hat{\gamma}_0(S)$	S	$\hat{\gamma}_1(S)$
$\bar{0}$	$0.\bar{0} = 0$	$\bar{1}$	$0.\bar{10} = \frac{2}{3}$
$\overline{01}$	$0.\overline{0110} = \frac{2}{5}$	$\overline{10}$	$0.\overline{1100} = \frac{4}{5}$
$\overline{101}$	$0.\overline{110} = \frac{6}{7}$	$\overline{110}$	$0.\overline{100} = \frac{4}{7}$
$\overline{100}$	$0.\overline{111000} = \frac{8}{9}$	$\overline{010}$	$0.\overline{011100} = \frac{4}{9}$
$\overline{1101}$	$0.\overline{10010110} = \frac{10}{17}$	$\overline{1011}$	$0.\overline{11010010} = \frac{14}{17}$
$\overline{1001}$	$0.\overline{1110} = \frac{14}{15}$	$\overline{0110}$	$0.\overline{0100} = \frac{4}{15}$
$\overline{1000}$	$0.\overline{11110000} = \frac{16}{17}$	$\overline{0010}$	$0.\overline{00111100} = \frac{4}{17}$
$\overline{11101}$	$0.\overline{10110} = \frac{22}{31}$	$\overline{10111}$	$0.\overline{11010} = \frac{26}{31}$
$\overline{10101}$	$0.\overline{1101100100} = \frac{26}{33}$	$\overline{10110}$	$0.\overline{1101100100} = \frac{28}{33}$
$\overline{10100}$	$0.\overline{11000} = \frac{24}{31}$	$\overline{10010}$	$0.\overline{11100} = \frac{28}{31}$
$\overline{11100}$	$0.\overline{1011101000} = \frac{8}{11}$	$\overline{10011}$	$0.\overline{1110100010} = \frac{10}{11}$
$\overline{10001}$	$0.\overline{11110} = \frac{30}{31}$	$\overline{00110}$	$0.\overline{00100} = \frac{4}{31}$
$\overline{10000}$	$0.\overline{1111100000} = \frac{32}{33}$	$\overline{00010}$	$0.\overline{0001111100} = \frac{4}{33}$

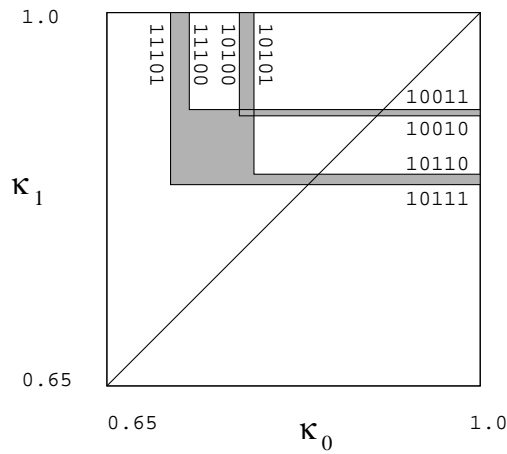


Figure 3. Bifurcation lines of the period 5 cycles yielding a bi-unimodal swallowtail ('crossroad area' [29, 5]) in the topological parameter plane (κ_0, κ_1) .

We can continue these calculations for longer cycles; the $\hat{\gamma}_s$ values for cycles up to length 5 are summarized in table 2. These values yield the bifurcation lines for the cycles in the topological parameter space (κ_0, κ_1) .

3.2. Bifurcation lines in the parameter plane

The bifurcation lines given by table 2 are easier to understand if we draw the lines in the (κ_0, κ_1) plane. The period 1, 2, 3, and 4 cycles yield single stable cycle bands. For each cycle only one maximum value is larger than $\frac{2}{3}$. We note that the $\bar{1}$, $\overline{10}$, and $\overline{1011}$ cycles bifurcate along constant κ_1 values, while $\overline{10\epsilon}$ and $\overline{100\epsilon}$ yield windows along constant κ_0 . We can find a similar structure for the Hénon map close to the $b = 0$ line.

However, the bi-unimodal approximation describes also more interesting higher codimension structures. The simplest example is given by the four period 5 cycles $\overline{10\epsilon_1 1\epsilon_2}$, $\epsilon_i \in \{0, 1\}$. The bifurcation lines for these cycles are drawn in figure 3. Each cycle exists

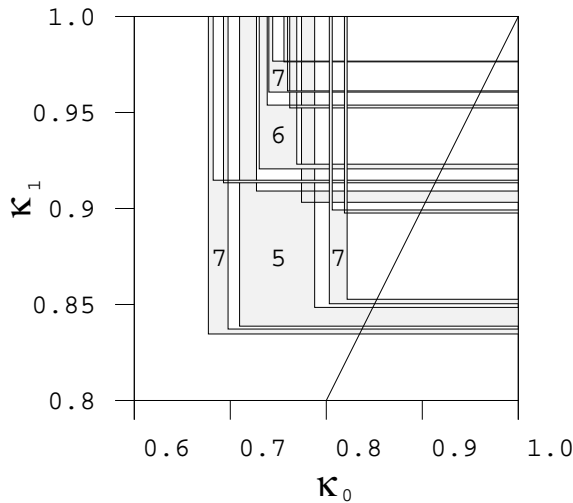


Figure 4. The topological parameter (κ_0, κ_1) bifurcation lines of the period 5, 6 and 7 swallowtails.

in a rectangle in the topological parameter plane. The inaccessible topological parameter values are shaded grey. The $\kappa_0 = \kappa_1$ line necessarily crosses the same stable windows $\overline{1011}\epsilon$ and $\overline{1001}\epsilon$ as the unimodal map, figure 1, but along the $\kappa_1 = 1$ line the cycles pair differently, as $\overline{1110}\epsilon$ and $\overline{1010}\epsilon$. We find in the (κ_0, κ_1) plane a topological structure which we shall refer to as a ‘swallowtail’, a parameter region within which the two pairs of cycles exchange partners. This structure is denoted a ‘crossroad area’ in [29, 5]. This swallowtail crossing is the distinctive feature of bi-unimodal maps; we shall illustrate it by finding all swallowtails for the short cycles up to length 9. If f_0 and f_1 are smooth functions then the function $f^{(5)}(x) - x$ will have the normal form $g = x^3 + ux + v$. Solving $g = 0$ for x , u , and v close to zero will depend on the two parameters u and v , and the dimensionality of the normal form parameter space (u, v) is called the codimension of the bifurcation [11]. Hence, the swallowtail such as the one illustrated in figure 3 is a codimension-2 bifurcation structure.

The bifurcation diagram for the period 6 cycles yields one swallowtail similar to the period 5 swallowtail with the symbolic dynamics given by $\overline{100\epsilon_01\epsilon_1}$. In the bi-unimodal approximation the other period 6 cycles yield simple windows with stable cycles. The period 7 cycles yield three different swallowtails in the topological parameter plane. The swallowtails for period 5, 6, and 7 cycles are drawn together in figure 4.

Longer cycles combine into increasing numbers of swallowtails. In figures 5(a) and (b) we display all swallowtail crossings for cycles of periods 8 and 9. The swallowtails are given by the following itineraries.

Period 5; $\overline{10\epsilon_01\epsilon_1}$.

Period 6; $\overline{100\epsilon_01\epsilon_1}$.

Period 7; $\overline{1000\epsilon_01\epsilon_1}$, $\overline{10\epsilon_0111\epsilon_1}$ and $\overline{10\epsilon_0101\epsilon_1}$.

Period 8; $\overline{10000\epsilon_01\epsilon_1}$, $\overline{100\epsilon_0101\epsilon_1}$, $\overline{100\epsilon_0111\epsilon_1}$, $\overline{10\epsilon_01011\epsilon_1}$ and $\overline{1001\epsilon_010\epsilon_1}$, where the last swallowtail lies below the diagonal and occurs for the orientation-preserving maps ($b < 0$ for the Hénon map).

Period 9; $\overline{100000\epsilon_01\epsilon_1}$, $\overline{1000\epsilon_0101\epsilon_1}$, $\overline{100\epsilon_01001\epsilon_1}$, $\overline{100\epsilon_01011\epsilon_1}$, $\overline{10\epsilon_011101\epsilon_1}$, $\overline{10\epsilon_010111\epsilon_1}$, $\overline{10\epsilon_010101\epsilon_1}$, $\overline{10\epsilon_011111\epsilon_1}$, $\overline{10011\epsilon_010\epsilon_1}$ and $\overline{10001\epsilon_010\epsilon_1}$ where the last two swallowtails exist for orientation-preserving maps.

Note that the figures describe both the number of swallowtails of different lengths and

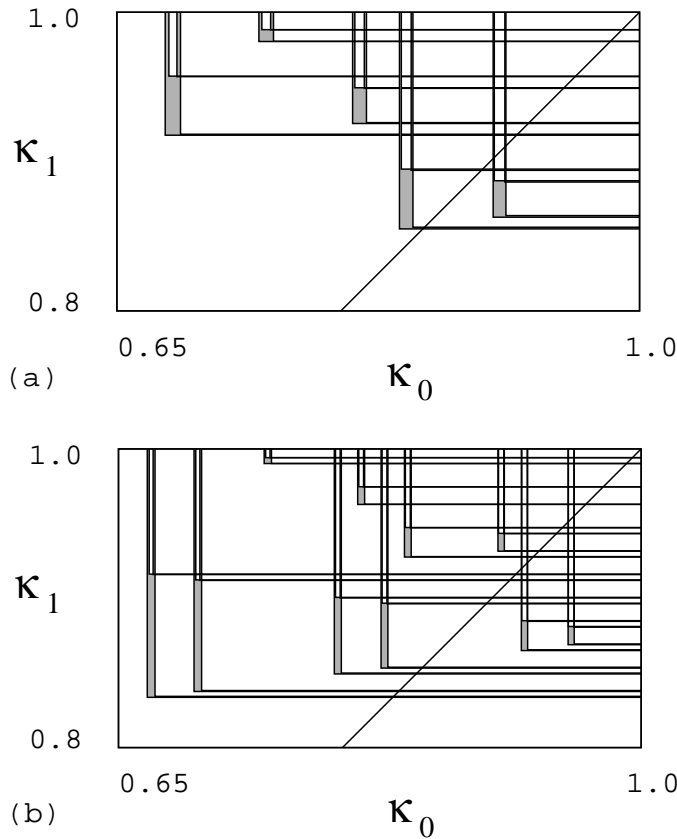


Figure 5. The bifurcation lines of the period (a) 8 and (b) 9 swallow tails in the topological parameter plane (κ_0, κ_1) .

their relative positions in the parameter plane. We observe that a number of swallowtails are ordered simply by rows and columns. For example, all swallowtails with the symbol strings $10^k\epsilon_01\epsilon_1$ with $k \in \{1, 2, \dots\}$ are placed above each other in the (κ_0, κ_1) plane, with each swallowtail nested in between the two tails of the swallowtail of the preceding shorter cycle, see figure 4.

The symbolic description for a generic swallowtail in the bi-unimodal approximation is given by the following proposition.

Proposition 1. *The four cycles that form a bi-unimodal swallowtail of an once-folding map have following itineraries:*

$$\bar{S} = \overline{s_1s_2 \cdots s_m 0\epsilon_0 s_{m+3}s_{m+4} \cdots s_{n-2} 1\epsilon_1} \tag{18}$$

with the kneading values

$$\begin{aligned} \hat{\gamma}_1(S) &= \gamma(\overline{s_1s_2 \cdots s_m 0\epsilon_0 s_{m+3}s_{m+4} \cdots s_{n-2} 1\epsilon_1}) \\ \hat{\gamma}_0(S) &= \gamma(\overline{s_{m+3}s_{m+4} \cdots s_{n-2} 1\epsilon_1 s_1s_2 \cdots s_m 0\epsilon_0}). \end{aligned} \tag{19}$$

The swallowtail crossing belongs to the orientation-reversing map ($b > 0$ for the Hénon map) if $\hat{\gamma}(\bar{S}) = \hat{\gamma}_1(\bar{S})$, and the orientation-preserving map ($b < 0$ for the Hénon map) if $\hat{\gamma}(\bar{S}) = \hat{\gamma}_0(\bar{S})$.

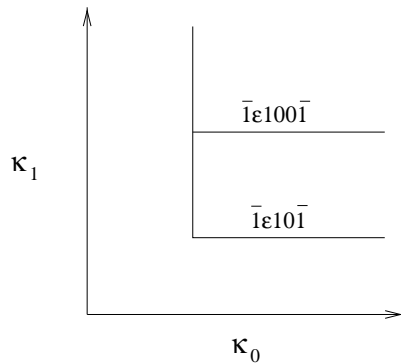


Figure 6. Bifurcation lines for the homoclinic orbits $\bar{1}\epsilon_010\epsilon_1\bar{1}$ in the topological parameter plane.

3.3. Aperiodic orbits

The aperiodic orbits have bifurcation structures in the bi-unimodal parameter plane similar to those discussed above, but the bifurcation structure of aperiodic orbits in one-dimensional bi-unimodal maps, discussed in [17], is more complicated than the bifurcation of periodic orbits. We will describe here briefly the bifurcation structures of some homoclinic orbits. The bifurcation lines of the four homoclinic orbits $\bar{1}\epsilon_010\epsilon_1\bar{1}$, with $\epsilon_0, \epsilon_1 \in \{0, 1\}$ are drawn in the topological parameter plane in figure 6. All four orbits have $\hat{\gamma}_0 = 0.\bar{1}0$, the two orbits $\bar{1}\epsilon_010\bar{1}$ have $\hat{\gamma}_1 = 0.1\bar{1}0$, and the two orbits $\bar{1}\epsilon_0100\bar{1}$ have $\hat{\gamma}_1 = 0.11\bar{1}0$. As shown in [17], there exists a complicated web of bifurcations connecting these bifurcation lines to other bifurcation lines in the parameter plane. The lines of crisis bifurcations and band merging are of this type.

4. Four-unimodal approximation

The bi-unimodal approximation developed above can explain most but not all of the bifurcation structures observed in the Hénon map (a, b) parameter plane discussed below. To explain further observed structures we have to refine the approximation and approximate the unstable manifold in figure 2(a) with four unimodal functions instead of just two as in figure 2(b). This four-unimodal reproduces all bifurcations of the unimodal and bi-unimodal approximations, and yields in addition more complicated bifurcation structures.

The choice of the branch at each iteration is now determined by the symbols of the two preceding points in the orbit $s_{-2}s_{-1}$, so we label the four functions by the four symbol strings f_{10}, f_{00}, f_{01} and f_{11} . The relative ordering of the four branches is given by the way the horseshoe map acts on the phase space, with the functions nested as $f_{10} < f_{00} < f_{01} < f_{11}$ for orientation-reversing maps (the Hénon map with $b > 0$) and as $f_{01} < f_{11} < f_{10} < f_{00}$ for the orientation-preserving maps (the Hénon map with $b < 0$).

Each map has a critical point with an associated topological parameter $\kappa_{s's}$ determined by the kneading sequence of its critical point. The relative ordering of $\kappa_{s's}$ is the same as of the functions themselves. For orientation-reversing maps

$$\kappa_{10} \leq \kappa_{00} \leq \kappa_{01} \leq \kappa_{11}, \tag{20}$$

and for orientation-preserving maps

$$\kappa_{01} \leq \kappa_{11} \leq \kappa_{10} \leq \kappa_{00}. \tag{21}$$

An orbit S now has four maximum values restricted to the four maps

$$\hat{\gamma}_{s's}(S) = \sup_m \gamma(\sigma^m(S)) \quad \text{with } s_{m-2} = s', s_{m-1} = s. \quad (22)$$

As in the bi-unimodal approximation, we can easily determine the $\hat{\gamma}_{s's}$ of all the short cycles, and study all possible bifurcations of orbits in the four-dimensional topological parameter space $(\kappa_{10}, \kappa_{00}, \kappa_{01}, \kappa_{11})$. Since we lack the ability to visualize three-dimensional bifurcations hyperplanes in a four-dimensional parameter space, we will draw bifurcation lines in the different two-dimensional topological parameter sections and some bifurcation planes in three-dimensional sections of the full parameter space. The six projections of the four-dimensional space into two-dimensional subspaces are $(\kappa_{10}, \kappa_{00})$, $(\kappa_{10}, \kappa_{01})$, $(\kappa_{10}, \kappa_{11})$, $(\kappa_{00}, \kappa_{01})$, $(\kappa_{00}, \kappa_{11})$, and $(\kappa_{01}, \kappa_{11})$. These projections will reveal the codimension-2 bifurcation structures possible in a generic once-folding map in the four-unimodal. We shall recover the unimodal and bi-unimodal structures already discussed above, together with some new bifurcation structures.

The projections of the four-dimensional topological parameter space into different two-dimensional spaces are non-trivial because of the ordering constraints (20) and (21). In simple one-dimensional tri-unimodal and four-unimodal maps [18] we can scan a two-dimensional topological parameter plane (κ_i, κ_j) while we let all the other topological parameter values have the extremum value that allows a maximum number of orbits. The two-dimensional planes give us all possible codimension-2 bifurcation structures in the system. For the four-unimodal maps discussed here we have drawn two-dimensional κ -planes where the other $\kappa_{s's}$ values are as large as possible but restricted by (20) and (21). The six planes are:

- $(\kappa_{10}, \kappa_{00})$ with $\kappa_{01} = \kappa_{11} = 1$ for $b > 0$ and $\kappa_{01} = \kappa_{11} = \kappa_{10}$ for $b < 0$,
- $(\kappa_{10}, \kappa_{01})$ with $\kappa_{00} = \kappa_{01}, \kappa_{11} = 1$ for $b > 0$ and $\kappa_{11} = \kappa_{10}, \kappa_{00} = 1$ for $b < 0$,
- $(\kappa_{10}, \kappa_{11})$ with $\kappa_{00} = \kappa_{01} = \kappa_{11}$ for $b > 0$ and $\kappa_{01} = \kappa_{11}, \kappa_{00} = 1$ for $b < 0$,
- $(\kappa_{00}, \kappa_{01})$ with $\kappa_{10} = \kappa_{00}, \kappa_{11} = 1$ for $b > 0$ and $\kappa_{11} = \kappa_{10} = \kappa_{00}$ for $b < 0$,
- $(\kappa_{00}, \kappa_{11})$ with $\kappa_{10} = \kappa_{00}, \kappa_{01} = \kappa_{11}$ for $b > 0$ and $\kappa_{01} = \kappa_{11}, \kappa_{10} = \kappa_{00}$ for $b < 0$,
- $(\kappa_{01}, \kappa_{11})$ with $\kappa_{10} = \kappa_{00} = \kappa_{01}$ for $b > 0$ and $\kappa_{10} = \kappa_{00} = 1$ for $b < 0$.

Here the Hénon map parameter b is used to indicate whether the map is orientation reversing or preserving.

Some of the assumed parameter limits, for example $\kappa_{00} = \kappa_{01} = \kappa_{11}$, are impossible in any smooth map. This introduces some unacceptable structures (see below), but ensures that we capture all possible codimension-2 structures existing in the four-dimensional parameter space. Inequalities (20) and (21) imply that the parameter planes $(\kappa_{10}, \kappa_{00})$, $(\kappa_{01}, \kappa_{11})$ only consist of the upper triangles $\kappa_{00} > \kappa_{10}$ and $\kappa_{11} > \kappa_{01}$ respectively and we do not know the sign of b in these planes. In the other four planes the diagonal corresponds to $b = 0$ in the Hénon map. The bifurcations lines are not necessarily continuous across the diagonal because the projections are different for $b > 0$ and $b < 0$. The four planes $(\kappa_{10}, \kappa_{01})$, $(\kappa_{10}, \kappa_{11})$, $(\kappa_{00}, \kappa_{01})$, and $(\kappa_{00}, \kappa_{11})$ (e.g. figures 8(b)–(e)) can be regarded as eight triangular planes drawn together for convenience.

4.1. Period 4 orbit cusp bifurcation

The shortest orbits which exhibit a new type of a codimension-2 singularity in the four-unimodal are the period 4 orbits 1000, 1001 and 1011. In figure 7 the bifurcation lines for these three orbits are drawn in the topological parameter plane $(\kappa_{10}, \kappa_{00})$. The unstable orbit 1001 is common in the two tails and at a point where the two tails meet this orbit yields a cusp bifurcation. This cusp is similar to the codimension-2 cusp in the centre of

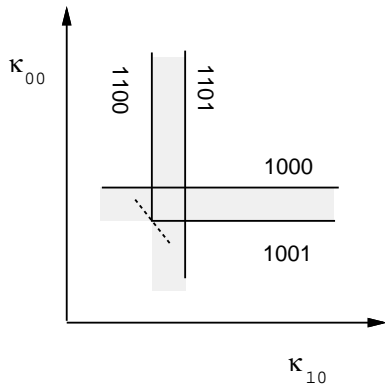


Figure 7. The bifurcation of the orbits $\overline{1000}$, $\overline{1001}$ and $\overline{1011}$ in the topological parameter plane $(\kappa_{10}, \kappa_{00})$.

Table 3. The four symbolic values κ_{10} , κ_{00} , κ_{01} and κ_{11} of the nine period 6 cycles.

κ_{01}	κ_{00}
$\tau(\overline{000010}) = 0.\overline{000011111100}$	$\tau(\overline{100000}) = 0.\overline{111111000000}$
$\tau(\overline{000011}) = 0.\overline{000010}$	$\tau(\overline{100001}) = 0.\overline{111110}$
$\tau(\overline{100011}) = 0.\overline{111101000010}$	$\tau(\overline{111000}) = 0.\overline{101111010000}$
$\tau(\overline{100010}) = 0.\overline{111100}$	$\tau(\overline{101000}) = 0.\overline{110000}$
$\tau(\overline{010011}) = 0.\overline{011101100010}$	$\tau(\overline{101001}) = 0.\overline{110001001110}$
$\tau(\overline{110011}) = 0.\overline{100010}$	$\tau(\overline{111001}) = 0.\overline{101110}$
$\tau(\overline{110010}) = 0.\overline{100011011100}$	$\tau(\overline{011001}) = 0.\overline{010001101110}$
$\tau(\overline{111011}) = 0.\overline{101101010010}$	—
$\tau(\overline{101011}) = 0.\overline{110010}$	—
κ_{10}	κ_{11}
$\tau(\overline{000100}) = 0.\overline{000111111000}$	—
$\tau(\overline{001100}) = 0.\overline{001000}$	$\tau(\overline{000110}) = 0.\overline{000100}$
$\tau(\overline{011100}) = 0.\overline{010111101000}$	$\tau(\overline{001110}) = 0.\overline{001011110100}$
$\tau(\overline{010100}) = 0.\overline{011000}$	—
$\tau(\overline{110100}) = 0.\overline{100111011000}$	$\tau(\overline{100110}) = 0.\overline{111011000100}$
$\tau(\overline{111100}) = 0.\overline{101000}$	$\tau(\overline{100111}) = 0.\overline{111010}$
$\tau(\overline{100101}) = 0.\overline{111001000110}$	$\tau(\overline{010110}) = 0.\overline{011011100100}$
$\tau(\overline{111101}) = 0.\overline{101001010110}$	$\tau(\overline{101111}) = 0.\overline{110101001010}$
$\tau(\overline{110101}) = 0.\overline{100110}$	$\tau(\overline{101110}) = 0.\overline{110100}$

the swallowtails discussed in the bi-unimodal case, but unlike a bi-unimodal swallowtail there is no connection to two other tails.

4.2. Period 6 swallowtails

It turns out that the period 5 orbits do not yield any new and interesting structures in the four-unimodal approximation. For the period 6 orbits we find four new codimension-2 structures.

All six topological parameter planes of period 6 orbits are drawn in figures 8(a)–(f). The symbolic values $\hat{\gamma}(S)$ used to draw these figures are given in table 3. We now discuss figure 8 in detail.

The period 6 swallowtail structure in figure 8(e) is the bi-unimodal swallowtail $\overline{100\epsilon_1 1\epsilon_2}$ already discussed and drawn in figure 4.

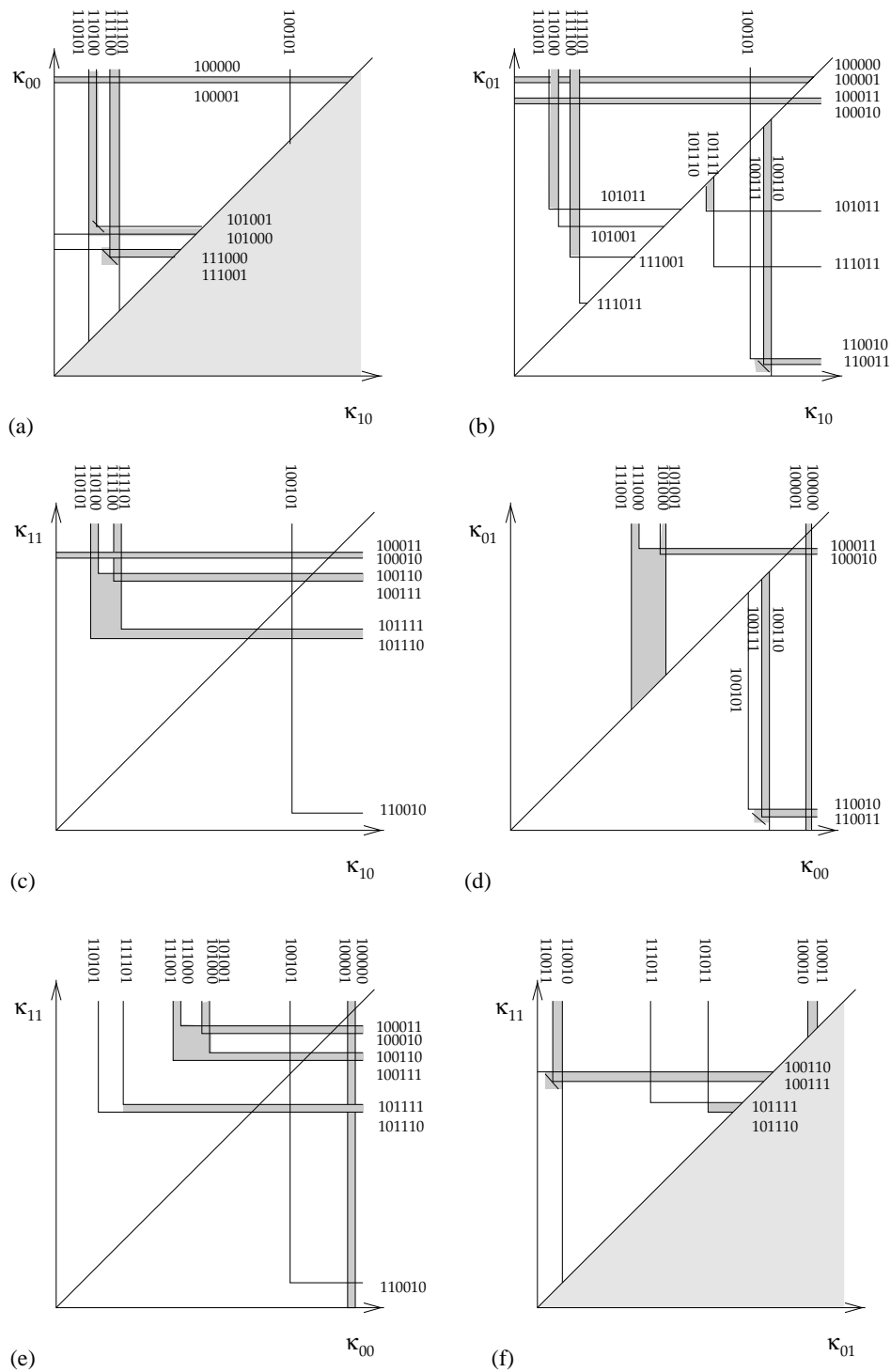


Figure 8. The bifurcation lines of period 6 orbits in the six four-unimodal topological parameter planes.

The swallowtail in figure 8(c) is a legal swallowtail of the once-folding map but one which we did not find in the bi-unimodal topological parameter plane. The symbolic description of the orbits in this swallowtail is $\overline{10\epsilon_1 11\epsilon_2}$.

Figure 8(a) illustrates some interesting new bifurcation structures. Here we find two cusp structures involving three orbits each. One cusp bifurcation involves the three orbits $\overline{111100}$, $\overline{111001}$, and $\overline{111101}$ while the other cusp involves the three orbits $\overline{101001}$, $\overline{101000}$, and $\overline{110101}$. The tail $\overline{11100\epsilon}$ bifurcating along the κ_{00} direction in figure 8(a) is also a tail bifurcating along the κ_{00} direction in figure 8(e) starting at the bi-unimodal swallowtail. We will focus on these structures because, as we shall see below, they are observed in the Hénon map.

In figure 8(f) we find a new cusp bifurcation involving the three orbits $\overline{100111}$, $\overline{100110}$, and $\overline{100101}$.

Figure 8(b) shows the topological parameter plane $(\kappa_{10}, \kappa_{01})$ and yields some unimodal structures and the cusp bifurcation also drawn in figure 8(f).

Figure 8(d) appears to be slightly more complicated but it contains no structures not already described above. A discontinuity at the diagonal $\kappa_{00} = \kappa_{01}$ is clearly visible here. At the diagonal the different folds switch ordering, so some bifurcation lines are discontinuous at this line in the symbol plane. This does not imply that there are any discontinuities in the Hénon map. The part of a swallowtail in the upper triangle here is the same bi-unimodal swallowtail as in figure 8(e) and not a new structure. The cusp in the lower triangle is the same cusp as in figure 8(f) and only a new image of this.

There are in addition some other topological bifurcation structures in figure 8 which cannot be interpreted as bifurcations. These do not give topological lines in pairs as required for a bifurcation in a dynamical system.

The interesting bifurcation planes can also be drawn in a three-dimensional parameter space. It turns out that the structure we get by combining the two swallowtails in figures 8(e) and 8(c) and the two cusps in figure 8(a) is of the same type as the bifurcation structure for the period 8 orbits discussed below in section 4.4, see figure 11.

4.3. Cusp bifurcations

The cusp bifurcation discussed above clearly shows the main problem that we face in defining symbolic dynamics for the Hénon-type maps. We illustrate this here in some detail by discussing one of the cusps. A conjecture of a universally valid definition of symbols in a Hénon map is stated elsewhere [16].

Figure 8(a) shows the cusp with the period 6 orbits $\overline{111000}$, $\overline{111001}$, and $\overline{111101}$, and figure 9 shows the stable and the unstable manifolds at the cusp point for the Hénon map. Our four-unimodal map cannot be a good description when one of the folds no longer have a turning point corresponding to a one-dimensional critical point. Figure 2(a) seems to justify a four-unimodal approximation, but figure 9 shows that we lose a tangency point close to the period 6 orbit for these parameter values. Closer examination of figure 9 shows that actually two of the folds lose their turning points corresponding to the critical points of the one-dimensional maps at the cusp and a proper approximation is then the bi-unimodal approximation with two unimodal maps. The problem is how to choose the symbol for a point on the fold that does not have a primary turning point. Moving in parameter space such that a turning point is created shows that there is not one unique point yielding the symbol partition, but the position of the point will depend on the path we choose in the parameter plane. This implies that orbits may change symbolic dynamics moving around the cusp in the parameter space as shown in [15] (see also [9]). The bifurcation lines for

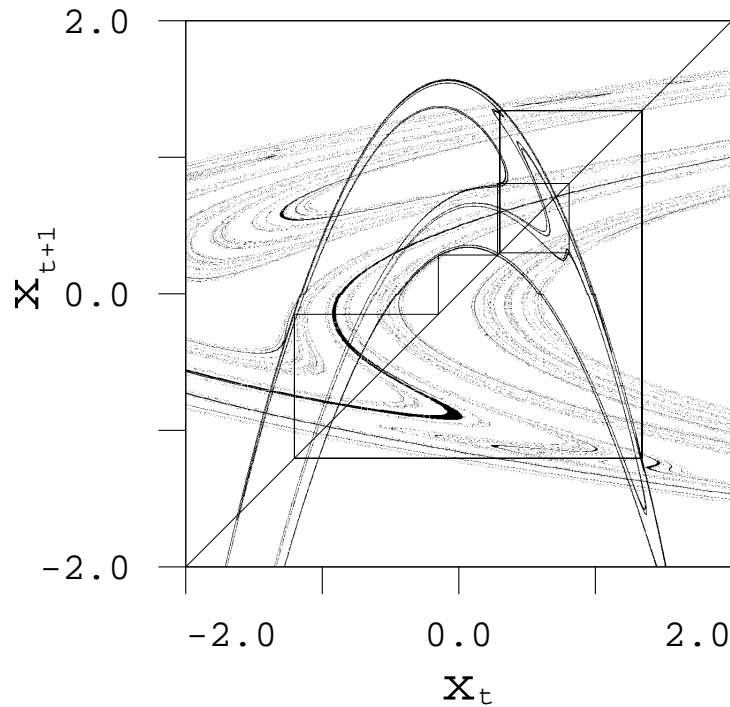


Figure 9. The stable and unstable manifolds at the cusp point for the period 6 orbit $\overline{100111}$.

$\overline{111000}$ and $\overline{111101}$ behind the cusp in figure 8(a) should therefore not be understood as bifurcation lines where an orbit is created in a dynamical system, but an indication of where the description of the orbit using the four-unimodal symbolic dynamics is correct. The orbit will also exist between the lines but without the same symbolic description in this approximation. The short diagonal lines on the cusps in figure 8 indicate the change from a four-unimodal to a bi-unimodal approximation.

The change of symbolic dynamics at a cusp also has consequences for the method proposed by Biham and Wenzel [3, 4] to find cycles in the Hénon map. As discussed in [16], there will be a region behind the cusp where the method does not converge.

The change in modality takes place when the critical point on the lower-most unimodal map iterates directly into the critical point of the second lower-most unimodal map. We can state this with symbolic dynamics using the kneading sequences of the maps.

Proposition 2. *In the four-unimodal there is a bifurcation from a four-unimodal to a bi-unimodal approximation of the once-folding map at parameter values where the kneading sequences of the maps satisfy the following condition; for order-reversing mapping ($b > 0$)*

$$K_{00} = \sigma(K_{10}), \quad (23)$$

for order-preserving mapping ($b < 0$)

$$K_{11} = \sigma(K_{01}). \quad (24)$$

Assuming $s_1 = 1$ for the kneading sequences we get the conditions on the topological parameter values for the bifurcation: for $b > 0$

$$\kappa_{00} = 2 - 2\kappa_{10}, \quad (25)$$

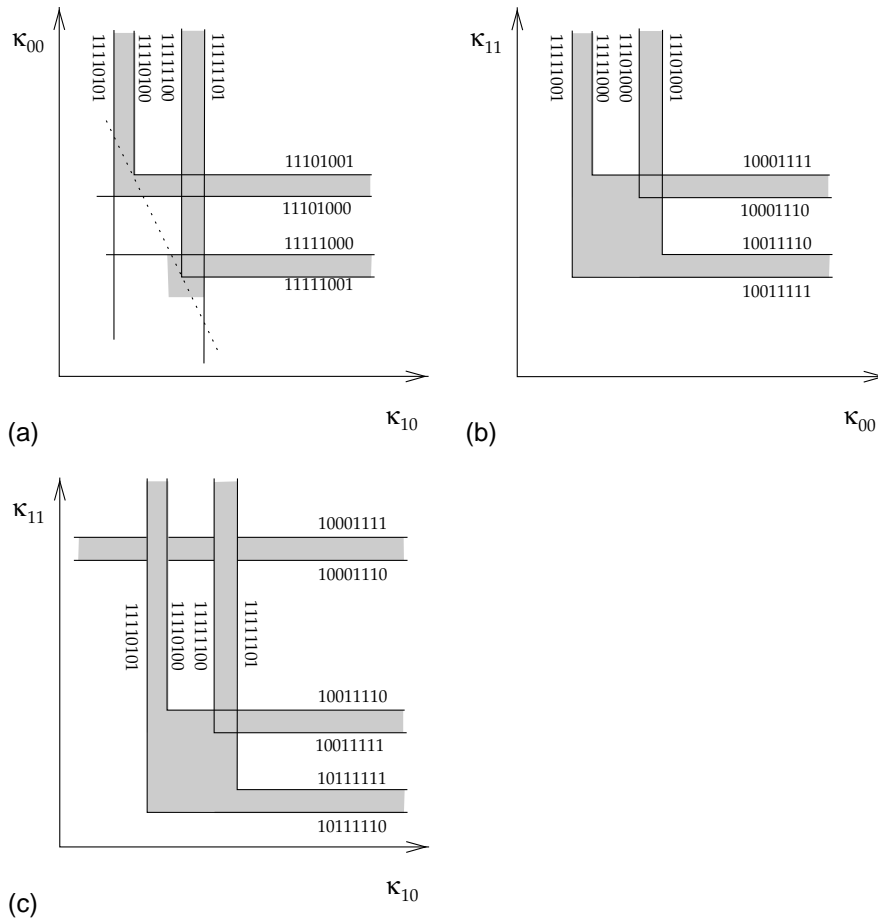


Figure 10. Bifurcation lines of some period 8 orbits in the two-dimensional projections of the topological parameter space (a) $(\kappa_{10}, \kappa_{00})$, (b) $(\kappa_{00}, \kappa_{11})$, (c) $(\kappa_{10}, \kappa_{11})$.

and for $b < 0$

$$\kappa_{11} = 2 - 2\kappa_{01}. \tag{26}$$

This requirement is satisfied for all the cusp points of the periodic orbits discussed above. One example is the cusp in figure 8(a) with the orbit $\overline{100111}$ giving $2 - 2\hat{\gamma}_{10}(\overline{100111}) = 2 - 2\gamma(\overline{111100}) = 2 - 2 \cdot 0.\overline{101000} = 2 - 1.0\overline{10001} = 0.\overline{101110} = \gamma(\overline{111001}) = \hat{\gamma}_{00}(\overline{100111})$. Depending on whether the number of 1's in the repeating string is odd or even, the stable orbit is either inside a cusp or it surrounds the cusp point of an unstable orbit.

4.4. Bifurcation of period 8 orbits

Another more complicated example of bifurcations observed in the Hénon map explainable by the four-unimodal approximation is the bifurcation structure of period 8 orbits. We therefore investigate the bifurcation structures in the topological parameter plane for the period 8 orbits.

In the same way as for the period 6 orbits we can construct two-dimensional topological parameter planes for all period 8 orbits. This will yield a very complicated picture; in

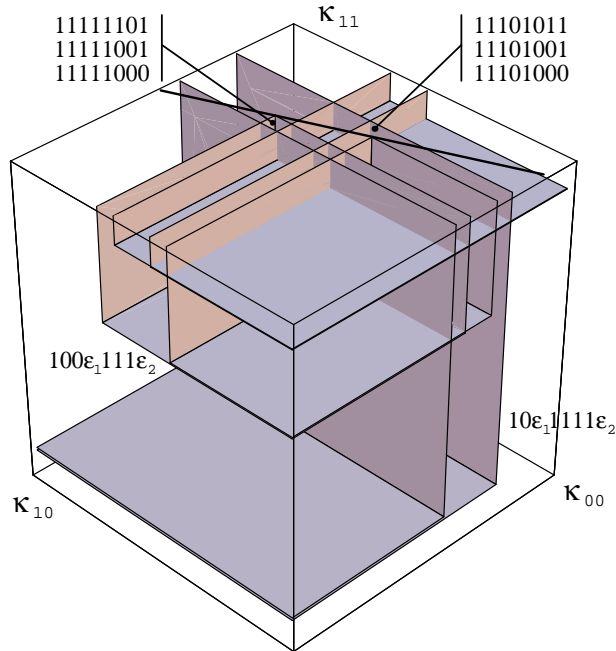


Figure 11. Bifurcation lines of some period 8 orbits in the three-dimensional topological parameter $(\kappa_{10}, \kappa_{00}, \kappa_{11})$.

figure 10 the bifurcation lines for some period 8 orbits are sketched in the three planes $(\kappa_{10}, \kappa_{00})$, $(\kappa_{00}, \kappa_{11})$, and $(\kappa_{10}, \kappa_{11})$. These drawings show that there are two cusp structures and two swallowtails in these topological parameter spaces quite similar to the period 6 orbits discussed above. One of the swallowtails is the swallowtail $100\epsilon_0111\epsilon_1$ from the bi-unimodal approximation (figure 5(a)), while the other structures appears only in the four-unimodal approximation.

We can combine the three pictures in figure 10 to draw a three-dimensional projection of the full four-dimensional topological parameter space. This will describe how the codimension-2 bifurcation structures are connected with stable windows in the parameter space. In figure 11 the exact bifurcation planes are drawn in the topological parameter space $(\kappa_{10}, \kappa_{00}, \kappa_{11})$. The ranges of the axes are $0.64 < \kappa_{10} < 0.69$, $0.67 < \kappa_{00} < 0.71$, and $0.82 < \kappa_{11} < 0.97$. The line $\kappa_{00} = 2 - 2\kappa_{10}$ yielding cusp structures equation (25) is also drawn. In this three-dimensional space the bifurcations take place at planes and an orbit exist inside a three-dimensional box with one corner at $(1, 1, 1)$. A scan of the (a, b) plane of the Hénon map corresponds to a two-dimensional hypersurface cutting through the bifurcation planes in this three-dimensional topological parameter space, yielding a bifurcation line whenever the (a, b) parameter hypersurface intersects the bifurcation plane of an orbit.

4.5. Area-preserving maps

The lines $|b| = 1$ in the Hénon map correspond to area-conserving maps. This limit is not a special line in the topological parameter space, but we can show that certain codimension-2 bifurcations require that the map is area conserving. To show this we have to use the symmetry between the stable and unstable manifolds.

To discuss this symmetry we first have to define a quantity for the stable manifold equivalent to $\gamma(S)$. This is given in [7, 6] as for $b > 0$

$$w_{t-1} = \begin{cases} 1 - w_t & \text{if } s_{t-1} = 0 \\ w_t & \text{if } s_{t-1} = 1 \end{cases} \quad w_0 = s_0$$

$$\delta(x) = 0.w_0w_{-1}w_{-2}\dots = \sum_{t=1}^{\infty} w_{1-t}/2^t, \tag{27}$$

and for $b < 0$

$$w_{t-1} = \begin{cases} w_t & \text{if } s_{t-1} = 0 \\ 1 - w_t & \text{if } s_{t-1} = 1 \end{cases} \quad w_0 = s_0$$

$$\delta(x) = 0.w_0w_{-1}w_{-2}\dots = \sum_{t=1}^{\infty} w_{1-t}/2^t. \tag{28}$$

From the pruning front conjecture [7, 6] it follows that since for area-preserving maps this is a symmetry between the unstable and stable manifolds it will also be a symmetry between the pruning fronts in γ and in δ . We can use this symmetry to discuss the cusp bifurcation.

At a cusp point singularity an orbit has two points on the pruning front corresponding to two cyclic permutations of the periodic symbol string; \bar{S} and $\bar{S}' = \sigma^k(\bar{S})$. The area-preserving map symmetry implies that the γ -values of these strings are symmetric to the δ -values of one backward shift of the same symbol string, as the area-preserving pruning front is symmetric to the backward iteration of the pruning front.

At a cusp in a two-dimensional parameter plane $(\kappa_{SS'}, \kappa_{S''S'''})$ the symbol string \bar{S} yields the value $\kappa_{SS'}$ and shifted string \bar{S}' yields the value $\kappa_{S''S'''}$. The cusp can only exist for the order-reversing area conserving map ($b = 1$) line if

$$\begin{aligned} \gamma(\bar{S}) &= 1 - \delta(\sigma^{-1}(\bar{S}')) \\ \delta(\bar{S}) &= 1 - \gamma(\sigma^{-1}(\bar{S}')) \\ \gamma(\bar{S}') &= 1 - \delta(\sigma^{-1}(\bar{S})) \\ \delta(\bar{S}') &= 1 - \gamma(\sigma^{-1}(\bar{S})) \end{aligned} \tag{29}$$

and for the order-preserving area conserving map ($b = -1$) if

$$\begin{aligned} \gamma(\bar{S}) &= \delta(\sigma^{-1}(\bar{S}')) \\ \delta(\bar{S}) &= \gamma(\sigma^{-1}(\bar{S}')) \\ \gamma(\bar{S}') &= \delta(\sigma^{-1}(\bar{S})) \\ \delta(\bar{S}') &= \gamma(\sigma^{-1}(\bar{S})) \end{aligned} \tag{30}$$

where σ^{-1} is the inverse shift operation of the symbol string, corresponding to an iteration once backward in time. This implies that the two periodic points on the pruning front in the symbol plane are symmetric to each other with respect to a symmetry line.

The cyclic permutations of the period 4 orbit 1001; $\bar{S} = 1001$ and $\bar{S}' = 1100$ yields $\kappa_{00} = \gamma(1001) = 0.1110$ and $\kappa_{10} = \gamma(1100) = 0.1000$, figure 7. Using the definitions (5)

and (27) we find the following relations between the symbolic values of the symbol string:

$$\begin{aligned}
 \gamma(\overline{1001}) &= 0.\overline{1110} = 1 - 0.\overline{0001} = 1 - \delta(\overline{0110}) = 1 - \delta(\sigma^{-1}(\overline{1100})) \\
 \delta(\overline{1001}) &= 0.\overline{1011} = 1 - 0.\overline{0100} = 1 - \gamma(\overline{0110}) = 1 - \gamma(\sigma^{-1}(\overline{1100})) \\
 \gamma(\overline{1100}) &= 0.\overline{1000} = 1 - 0.\overline{0111} = 1 - \delta(\overline{1100}) = 1 - \delta(\sigma^{-1}(\overline{1001})) \\
 \delta(\overline{1100}) &= 0.\overline{0111} = 1 - 0.\overline{1000} = 1 - \gamma(\overline{1100}) = 1 - \gamma(\sigma^{-1}(\overline{1001})).
 \end{aligned} \tag{31}$$

This is the symmetry relation (29) corresponding to the Hénon map with $b = 1$.

The cusp of the period 6 orbits with the orbits $\overline{101001}$, $\overline{101000}$, and $\overline{110101}$ has the orbit $\overline{101001}$ common in the two tails with the cyclic permutations $S = \overline{101001}$ and $S' = \overline{110100}$ giving the symbolic values κ_{00} and κ_{10} at the singular point. Direct calculation using definitions (5) and (27) yields

$$\begin{aligned}
 \gamma(\overline{101001}) &= 1 - \delta(\sigma^{-1}(\overline{110100})) \\
 \delta(\overline{101001}) &= 1 - \gamma(\sigma^{-1}(\overline{110100})) \\
 \gamma(\overline{110100}) &= 1 - \delta(\sigma^{-1}(\overline{101001})) \\
 \delta(\overline{110100}) &= 1 - \gamma(\sigma^{-1}(\overline{101001})),
 \end{aligned}$$

the symmetry in (29) which restricts the cusp to the $b = 1$ line.

There is a cusp structure for period 6 orbits involving the three orbits $\overline{100111}$, $\overline{100110}$, and $\overline{110010}$. The common orbit in the two tails are $\overline{100111}$ and the cyclic permutations $S = \overline{100111}$ and $S' = \overline{110011}$ gives the symbolic values κ_{11} and κ_{01} at the singular point. Using the definitions (5) and (28) for $b < 0$ we find

$$\begin{aligned}
 \gamma(\overline{100111}) &= \delta(\sigma^{-1}(\overline{110011})) \\
 \delta(\overline{100111}) &= \gamma(\sigma^{-1}(\overline{110011})) \\
 \gamma(\overline{110011}) &= \delta(\sigma^{-1}(\overline{100111})) \\
 \delta(\overline{110011}) &= \gamma(\sigma^{-1}(\overline{100111}))
 \end{aligned}$$

which is the symmetry equation (30) for the Hénon map at $b = -1$.

5. Hénon map bifurcations

We shall now try to verify the bifurcation structure described above for a generic topological parameter space in the specific parameter space (a, b) of the Hénon map. The different bifurcation lines and many of the swallowtails in the bi-unimodal approximation can be found numerically in this (a, b) plane. Many of these bifurcation structures have been drawn in e.g. [8, 29].

The bifurcation curves for the cycles with period 1, 2, 3 and 4 for $|b| < 1$ give only simple windows similar to the bifurcation lines obtained in the topological parameter space.

In figure 12 we have drawn the bifurcation lines for the period 4 orbits in the parameter plane (a, b) close to the $b = 1$ line. We find here the cusp predicted in the topological parameter plane. In agreement with the arguments above, we do find that the cusp point is exactly on the $b = 1$ line.

A scan of the (a, b) plane for the Hénon map, searching for stable period 5 orbits reveals the swallowtail bifurcation as drawn in figure 13. We notice that in figure 3 the swallowtail crossing in the symbol plane takes place for $\kappa_1 > \kappa_0$, corresponding to an orientation-reversing horseshoe, that is $b > 0$ for the Hénon map. The period doubling to two period 10 swallowtail crossings, four period 20 crossings etc, is found for the Hénon map exactly

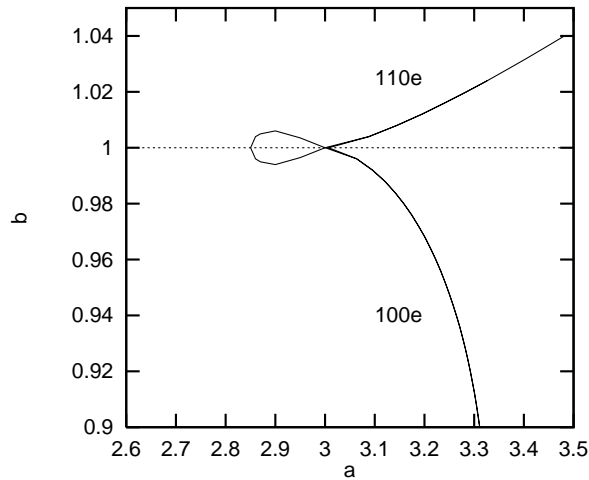


Figure 12. The bifurcation curves of the period 4 orbits in the Hénon map.

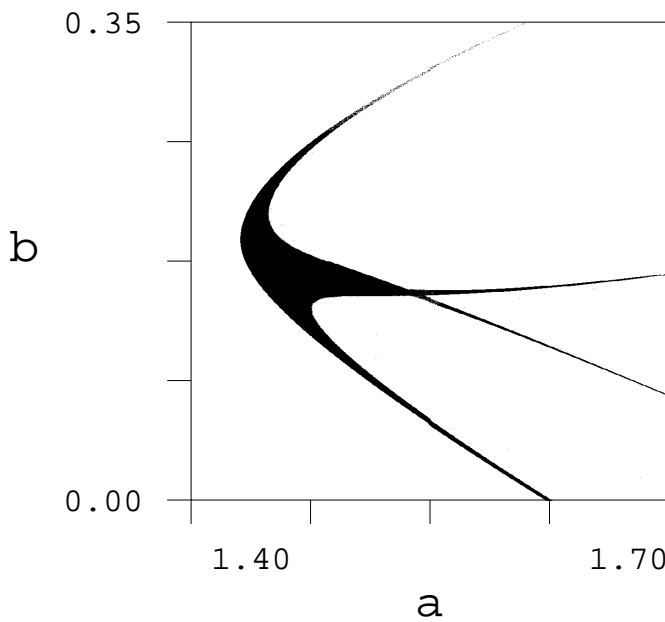


Figure 13. The swallowtail of period 5 orbits in the parameter plane (a, b) for the Hénon map: areas with stable period 5 orbit.

as constructed in the bi-unimodal map symbol plane [16]. This bi-unimodal bifurcation structure is the same as the well studied one-dimensional bimodal maps in [23–25, 10, 27].

The relative position between two swallowtails in the topological parameter plane is a topological feature which is valid also in any 2-parameter plane (a, b) for a once-folding map. If one swallowtail crossing is between two other tails in the topological parameter plane or if a tail from one swallowtail crosses a tail from a different swallowtail, then this will be true also in a (a, b) parameter plane.

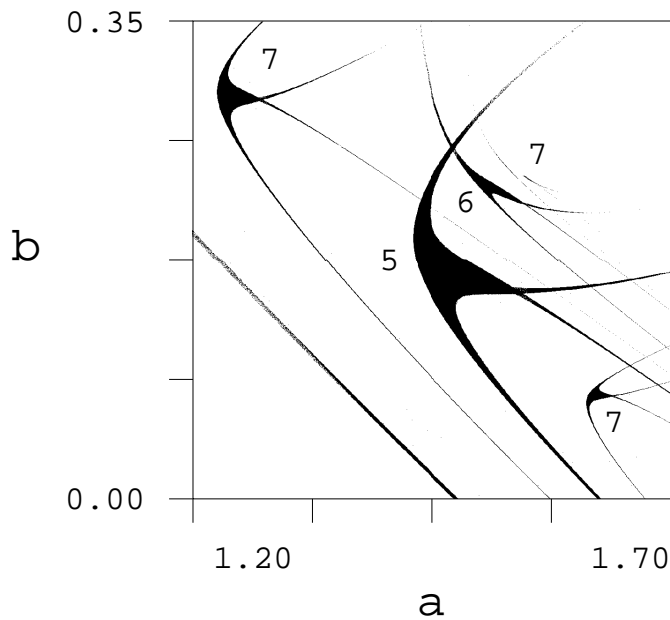


Figure 14. Swallowtails in the Hénon map: areas in the (a, b) parameter plane corresponding to stable period 5, 6 or 7 orbit are marked in black.

We now compare the bi-unimodal admissible swallowtails of the short orbits with the swallowtails realized by the Hénon map. In figure 4 the swallowtails for period 5, 6 and 7 are drawn together in the topological parameter plane. Observe the topological structure; which tails that cross other tails and which swallowtails are nested within other swallowtails. There is one horizontal row of period 7, 5 and 7 swallowtails and there is one vertical column with period 5, 6 and 7 swallowtails. Figure 14 is a scan of the (a, b) plane of the Hénon map, with the areas corresponding to stable period 5, 6 and 7 orbits are marked in black. The swallowtails are arranged topologically as in figure 4, with only a few differences in the structure. One of the tails from the period 6 swallowtail crosses a tail of the period 5 swallowtail; according to the bi-unimodal topological parameter plane this should not occur. As we will discuss below, this arises from the four-unimodal approximation. Also the period 7 swallowtail above the period 6 swallowtail has one tail crossing a period 5 tail. This period 7 swallowtail $\overline{1000\epsilon_0 1\epsilon_1}$ is not a complete swallowtail but is broken up into a cusp and an isolated tail. The bifurcation lines are correctly described by the bi-unimodal topological parameter plane but because the tails bifurcate on different folds with a finite distance the orbit is not stable in the whole region where the bi-unimodal map is stable.

In figure 15 we find that one of the tails from the swallowtail $\overline{100\epsilon_0 1\epsilon_1}$ is connected to a cusp bifurcation. This is the bifurcation predicted by figures 8(a) and (e). In both figures 8(a) and (e) the tail $\overline{11100\epsilon}$ bifurcates at a κ_{00} value. The tail is connected to the swallowtail $\overline{100\epsilon_0 1\epsilon_1}$ in figure 8(e) and to the cusp with the orbits $\overline{111000}$, $\overline{111001}$, and $\overline{111101}$ in figure 8(a). This is the tail connecting the two codimension-2 structures in the (a, b) plane in figure 15.

Another connection between codimension-2 structures predicted from figures 8(a) and (e) is the tail $\overline{10100\epsilon}$ which connect the swallowtail $\overline{100\epsilon_0 1\epsilon_1}$ with the cusp consisting of the orbits $\overline{101001}$, $\overline{101000}$, and $\overline{110101}$. We have found above that this cusp has the symmetry

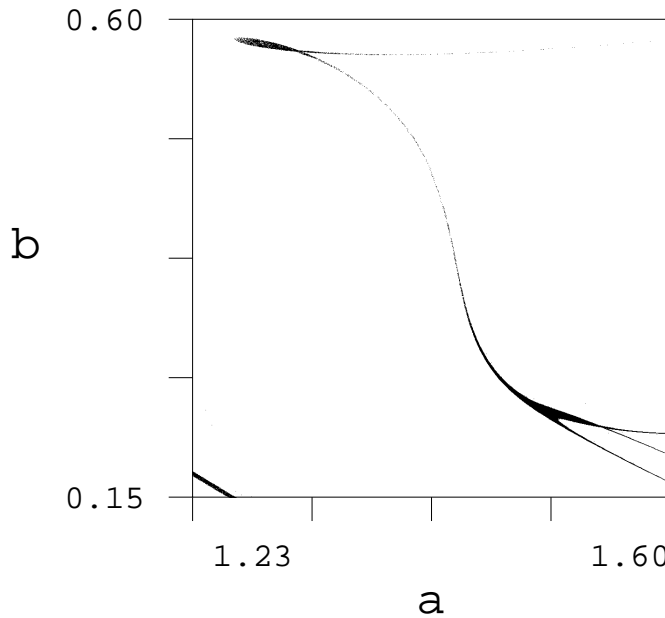


Figure 15. The (a, b) parameter plane regions with a stable period 6 orbit in the Hénon map.

restricting it to the $b = 1$ line. Numerically the cusp is found at $a \approx 2.75, b = 1$.

The third cusp in figure 8(f) with the orbits $\overline{100111}$, $\overline{100110}$, and $\overline{110010}$ is predicted to be connected to the bi-unimodal swallowtail with the tail $\overline{10011\epsilon}$ and exist at the $b = -1$ line. Numerically this cusp is found at $a \approx 3.0, b = -1$.

The swallowtail in figure 8(c) is not found for the Hénon map. It uses some of the same orbits as the other codimension-2 structures and it will therefore be difficult to have this together with the other structures in the same (a, b) plane. This cusp is realized by other once-folding maps; it has been found in the two-dimensional Lozi map [22, 16].

The bifurcations of the period 8 orbits turns out to be the most complicated of the short cycles. The period 8 swallowtails in figure 5(a) with symbolic description $\overline{100\epsilon_0111\epsilon_1}$ do not exist for the Hénon map but can exist for a slightly perturbed Hénon map. In the four-unimodal approximation this swallowtail is in figure 11 connected to one other swallowtail and two cusps. To show that the rather strange-looking bifurcation we find for the Hénon map is described by the bifurcation planes in figure 11 we study a variation of the Hénon map where we add a x^4 term with a third parameter c :

$$x_{t+1} = 1 - ax_t^2 - cx_t^4 + bx_{t-1}. \tag{32}$$

This map is once-folding for $c > 0$. For $c < 0$ the map is in principle thrice-folding, but close to $c = 0$ the map behaves like a once-folding map for small values of x .

Figure 16 shows the parameter values with a stable period 8 orbit for the perturbed Hénon map (32). For $c = 0$, figure 16(c), this is the Hénon map. We find in figure 16 that the bifurcation structures changes smoothly with the new parameter c and for $c = 0.08$ and for $c = -0.06$ we find combinations of familiar codimension-2 structures, swallowtails and cusps, while for $c = 0$ a more complicated structure emerges.

The (a, b) plane in figure 16(a) corresponds to a plane that cuts through the two cusps on the top and through the swallowtail on the left-hand side of figure 11. This is the structure

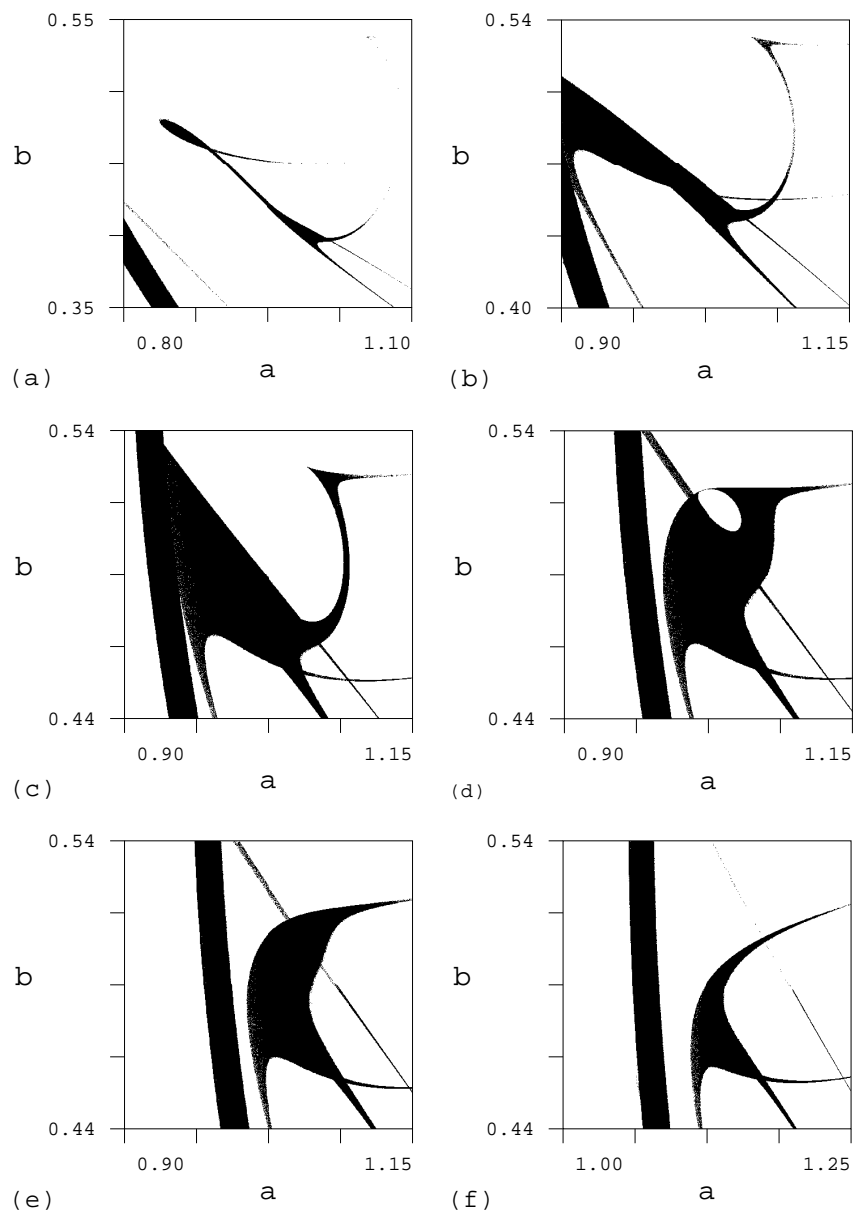


Figure 16. The parameter values giving stable period 8 orbits in the perturbed Hénon map (32) in the parameter space (a, b) with different values of c . (a) $c = 0.08$, (b) $c = 0.02$, (c) $c = 0$ (the Hénon map), (d) $c = -0.013$, (e) $c = -0.02$, (f) $c = -0.06$.

drawn in figures 10(a) and (c). The (a, b) plane in figure 16(f) corresponds to a plane that only cuts through the swallowtail on the right-hand side of figure 11 (figure 10(b)). The Hénon map in figure 16(c) is a plane cutting through the structure in the middle of figure 11 where the swallowtails and the cusps merge together. This illustrates a true codimension-3 bifurcation for maps of the Hénon type.

The reader is referred to works of Mira [29] and Carcassés [5] for a detailed study giving

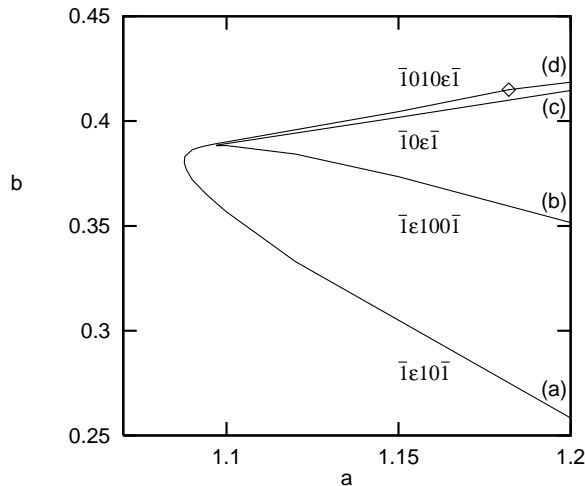


Figure 17. The bifurcation lines of some homoclinic orbits of the Hénon map in the parameter plane (a, b) . The labels indicate the parameter values in figure 18.

more examples of bifurcation structures in the Hénon map.

We have shown here how the bifurcations in the Hénon map can be understood if we extend the map with a third parameter and consider the bifurcations as a structure in a three-dimensional (a, b, c) parameter space. With this procedure we find a complete agreement between the predictions of the topological parameter space and the numerics. Hence the proper way to study bifurcations of cycles in the Hénon map is to extend the investigation to an infinite-dimensional topological parameter space of all ‘Hénon-like’ maps.

5.1. Aperiodic orbits

The bifurcation of homoclinic orbits in a smooth bi-unimodal map would give bifurcation lines similar to the bifurcation lines in the symbol plane, figure 6, as discussed in [17].

The bifurcation lines in the Hénon map for the homoclinic orbits with symbolic description $\overline{1\epsilon_0 10\epsilon_1 1}$ are drawn in figure 17. The bifurcation line $\overline{1\epsilon 10 1}$ is where the attractor merges from two parts into one connected attractor. This is analogous to the band-merging bifurcations in a unimodal map. This bifurcation takes place along the curve $\overline{1\epsilon 10 1}$ (figure 18(a)) until the cusp area and from the cusp area along the line $\overline{1010\epsilon 1}$ until the marker in figure 17. Above this point there is a different homoclinic tangency, the line $\overline{1\epsilon 1000 1}$, which is the border between two or one connected chaotic attractor. The other bifurcation curves are other homoclinic bifurcations as illustrated in figures 18(b)–(d). The bifurcation curves have similar shapes as in the topological parameter plane (figure 6), but the bifurcation curve corresponding to the $\kappa_0 = 0.\overline{10}$ line is split into two curves and one of the curves has a cusp. The cusp is not as narrow as the homoclinic orbit cusp one finds in bi-unimodal maps [17]. Numerically it seems to be the same type of cusp as we have in the centre of the swallowtail where the width of the cusp increases as the distance to the power $\frac{3}{2}$. The second smooth curve in figure 17 seems to lack the singularity in the derivative found for bi-unimodal maps [17].

The homoclinic orbits are changing the symbolic description in the neighbourhood of the cusp point. We find that the homoclinic orbit $\overline{10 1}$ bifurcates at point (a) and (c) in

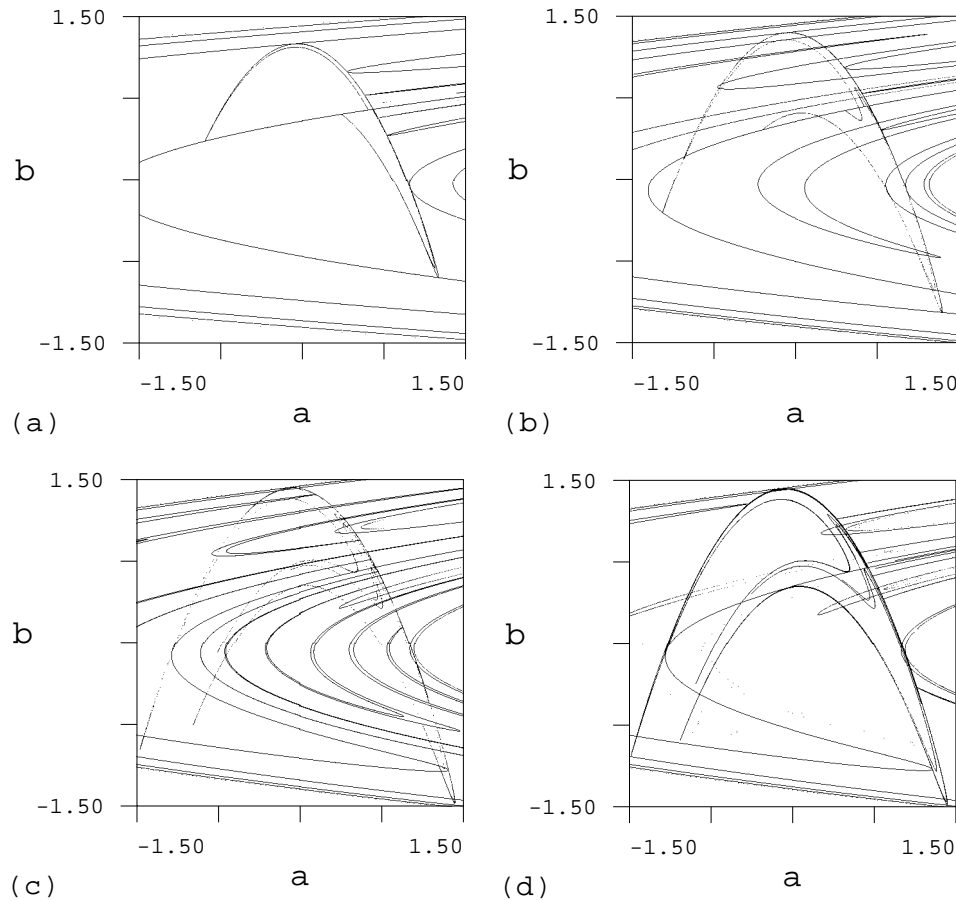


Figure 18. Homoclinic bifurcations in the Hénon map at parameter values indicated in figure 17. (a) $\overline{1\epsilon 10\overline{1}}$ for $a = 1.2$, $b = 0.25838$. (b) $\overline{1\epsilon 100\overline{1}}$ for $a = 1.2$, $b = 0.3516$. (c) $\overline{10\epsilon\overline{1}}$ for $a = 1.2$, $b = 0.4146037$. (d) $\overline{1010\epsilon\overline{1}}$ for $a = 1.2$, $b = 0.418569132$.

figure 17 but there is no bifurcation curve connecting these two points. The orbits therefore have to change symbolic dynamics at some point along the bifurcation line.

The bi-unimodal approximation fails to predict the splitting of the bifurcation curve, $\kappa_0 = 0.\overline{10}$, and only predicts the main structure. To explain this we have to take into account that the map is two-dimensional with smooth stable and unstable manifolds. This is a point where the two-dimensionality of the map is important.

In contrast to the periodic orbits, bifurcation lines of homoclinic orbits in the symbol plane yield bifurcations of an infinite number of different orbits. In a bi-unimodal map this gives a fractal set of singular bifurcation points on these bifurcation lines and a complicated web through the parameter space. In the two-dimensional folding map the degenerated bifurcation line of the one-dimensional map splits into a Cantor set collection of bifurcation lines, one line for each pair of the infinite number of aperiodic orbits.

6. Monotonicity

In the four-dimensional topological parameter space of the four-unimodal approximation discussed here there are many one-dimensional parameter lines along which orbits are only created and not destroyed. Along all curves $C(\kappa)$ in $(\kappa_{10}, \kappa_{00}, \kappa_{01}, \kappa_{11})$ where $\partial C / \partial \kappa_{ss'} \geq 0$ the non-wandering set will be constant or increase as κ increases. Consequently the topological entropy will not decrease along such curves. From a given point in the topological parameter space one can construct a four-dimensional cone containing these curves such that the cone separates the region where all four topological parameter values are larger from the region where all four topological parameter values are smaller than the starting point.

A similar statement can be made for the two-dimensional parameter plane (κ_0, κ_1) and for the 8, 16, 32, ...-dimensional parameter spaces for the higher-order approximations. Our description therefore gives a monotone map in the sense that through any point in the parameter plane one can find a one-dimensional curve along which the bifurcations only create orbits. There also exist of course paths along which orbits are both created and destroyed.

A difficult question is whether this monotonicity property of the $(\kappa_{10}, \kappa_{00}, \kappa_{01}, \kappa_{11})$ space carries over to a given four-dimensional parameter space (a, b, c, d) describing a specific map, say the Hénon map. As we have showed above in a number of examples, the description of bifurcation of periodic orbits and homoclinic orbits seems to be the same in the two parameter spaces. We also believe that the property of monotonicity is true in a typical (a, b, c, d) parameter space for a once-folding map. This implies that from any given point in the parameter space there originates a four-dimensional cone within which all curves $\tilde{C}(a)$ yield non-wandering sets of increasing topological entropy. In the most extreme points (cusp bifurcation points) this cone may shrink to a line, but should always exist. For the Hénon map which only has two parameters there may exist points from where there are no curves $\tilde{C}(a, b)$ along which orbits are only born, but by introducing more parameters it should be possible to find such a curve $\tilde{C}(a, b, c, d, \dots)$. One example is figure 16(d) where we have a region in (a, b) bounded by a curve creating a stable period 8 orbit. All curves in this (a, b) plane for $c = -0.013$ have to cut the bifurcation line twice and are not monotone. However, a line which has fixed (a, b) and a varying value of c will be monotone with respect to the period 8 orbit. This codimension-3 structure has the monotonicity in a cone in the (a, b, c) parameter space for the extended Hénon map.

In a general 2^n approximation it will be a 2^n -dimensional cone from a point in the 2^n -dimensional topological parameter space in which the non-wandering set is increasing. We believe that in a corresponding 2^n -dimensional parameter space (a, b, c, \dots, z) describing a particular map, there is also a cone with a monotone increasing non-wandering set.

These arguments are in disagreement with the paper of Kan *et al* [21] which claims that there does not exist any curve in the parameter plane along which orbits are only created, and none are destroyed. The validity of this theorem has been questioned in [19].

7. Discussion and conclusions

The most crucial question about our description is whether symbolic dynamics is at all uniquely defined for a system like the Hénon map. This has been discussed by Grassberger and Kantz [12, 13] who introduced 'primary turning points' in order to partition the non-wandering set of the Hénon map, and by Cvitanović *et al* [7] whose pruning front is conjectured to provide such partition. All numerical studies indicate that such symbolic

dynamics does exist. It has also been claimed that a unique symbolic dynamics for the Hénon map can be defined for any given parameter values [16]. Biham and Wenzel [3, 4] introduced a useful method for numerical determination of periodic orbits, which, when the method converges, also assigns unique symbolic itinerary to each periodic orbit. Unfortunately, as explained above, this method does not converge in regions of the (a, b) plane behind cusps, where unstable orbits change their symbolic description.

The next question is whether the choice of a bi-unimodal, four-unimodal, etc approximation is valid, and if valid whether it is useful. An alternative way to present the method would be to say that we approximated the pruning front [7] by 2 steps, 4 steps, etc. We find that the geometry of the problem makes the multi-unimodal approximations very natural, and tracing the bifurcation structures in higher codimension topological parameter spaces yield a more systematic and powerful approach than what has been done so far, in studies restricted to two-dimensional parameter hypersurfaces.

The existence of a map to and from the topological parameter space to a parameter plane (a, b) for the Hénon map remains an unproven conjecture. There are many other aspects of this problem where deeper understanding is still lacking, but the predictions based on multi-unimodal approximations agree with the numerics for the Hénon map in so far as we have tested them. We believe that the description of bifurcation structures obtained here contributes to the understanding of the Hénon and other maps of this type.

Acknowledgments

We are grateful to V Baladi, B Brenner, A de Carvalho, J Frøjlund, P Grassberger, J Guckenheimer, G H Gunaratne, P J Holmes, J Milnor, I Procaccia, D Sullivan, and C Tresser for stimulating discussions. PC is grateful to M J Feigenbaum for providing inspiration, criticism and protective shelter through all stages of this project and the Carlsberg Foundation for the support. KTH thanks the Norwegian Research Council and NORDITA for support, and Niels Bohr Institute for hospitality.

References

- [1] D'Alessandro G, Grassberger P, Isola S and A Politi 1990 *J. Phys. A: Math. Gen.* **23** 5285
- [2] Benedicks M and Carleson L 1991 *Ann. Math.* **133** 73
- [3] Biham O and Wenzel W 1989 *Phys. Rev. Lett.* **63**, 819
- [4] Biham O and Wenzel W 1990 *Phys. Rev. A* **42** 4639
- [5] Carcassés J P 1993 Determination of different configurations of fold and flip *Int. J. Bifurcations Chaos* **3** 869
- [6] Cvitanović P 1991 *Physica D* **51** 138
- [7] Cvitanović P, Gunaratne G H and Procaccia I 1988 *Phys. Rev. A* **38** 1503
- [8] Fournier D, Kawakami H and Mira C 1984 *C. R. Acad. Sci. I* **298** 253
Fournier D, Kawakami H and Mira C 1985 *C. R. Acad. Sci. I* **301** 223
Fournier D, Kawakami H and Mira C 1985 *C. R. Acad. Sci. I* **301** 325
- [9] Giovannini F and Politi A 1992 *Phys. Lett. A* **161** 333
- [10] Glass L and Perez R 1982 *Phys. Rev. Lett.* **48** 1772
- [11] Golubitsky M and Schaeffer D G 1985 *Singularities and Groups in Bifurcation Theory (Applied Mathematical Sciences 51)* (Berlin: Springer)
- [12] Grassberger P and Kantz H 1985 *Phys. Lett. A* **113** 235
- [13] Grassberger P, Kantz H and Moening U 1989 *J. Phys. A: Math. Gen.* **43** 5217
- [14] Guckenheimer J 1977 *Inventions. Math.* **39** 165
- [15] Hansen K T 1992 *Phys. Lett. A* **165** 100
- [16] Hansen K T 1993 Symbolic dynamics in chaotic systems *PhD Thesis* University of Oslo
<http://www.nbi.dk/CATS/papers/khansen/thesis/thesis.html>
- [17] Hansen K T 1994 *Phys. Rev. E* **50** 1653

- [18] Hansen K T Bifurcation structures for multimodal maps *Preprint*
http://alf.nbi.dk/CATS/papers/multi_mod.ps.gz
- [19] Hansen K T 1996 *Preprint* <http://www.nbi.dk/CATS/papers/anti/anti.html>
- [20] Hénon M 1976 *Commun. Math. Phys.* **50** 69
- [21] Kan I, Koçak H and Yorke J 1992 *Ann. Math.* **136** 219
- [22] Lozi R 1978 *J. Phys. Paris Colloq.* **39** 9
- [23] MacKay R S and Tresser C 1986 *Physica D* **19** 206
- [24] MacKay R S and Tresser C 1987 *Physica D* **27** 412
- [25] MacKay R S and van Zeijts J B J 1988 *Nonlinearity* **1** 253
- [26] Metropolis N, Stein M L and Stein P R 1973 *J. Comb. Theor. A* **15** 25
- [27] Milnor J 1992 *Exp. Math.* **1** 5
- [28] Milnor J and Thurston W 1988 *Lecture Notes in Mathematics* vol 1342 (Berlin: Springer) p 465
- [29] Mira C 1987 *Chaotic Dynamics* (Singapore: World Scientific)
- [30] Myrberg P J 1958 *Ann. Acad. Sci. Fenn. A* **259** 1
- [31] Sarkovskii A N 1964 *Ukrainian Math. J.* **16** 61
- [32] Simo S 1979 *J. Stat. Phys.* **21** 465
- [33] Smale S 1967 *Bull. Am. Math. Soc.* **73** 747